



Greenhouse gas measurement campaign of the Earth Summit Mission-2022: ground-based *in situ* and FTIR observations and contribute to satellite validation in the Qomolangma region

Minqiang Zhou^{1,3}, Yilong Wang^{2,3*}, Minzheng Duan^{3,4*}, Xiangjun Tian^{2,3}, Jinzhi Ding^{2,3}, Jianrong Bi⁵, Yaoming Ma^{2,6}, Weiqiang Ma^{2,6}, Zhenhua Xi^{2,6}

¹ *State Key Laboratory of Atmospheric Environment and Extreme Meteorology, Institute of Atmospheric Physics, Chinese Academy of Sciences, Beijing 100029, China*

² *State Key Laboratory of Tibetan Plateau Earth System, Environment and Resources, Institute of Tibetan Plateau Research, Chinese Academy of Sciences, Beijing 100101, China*

³ *University of Chinese Academy of Sciences, Beijing 100049, China*

⁴ *Key Laboratory for Middle Atmosphere and Global Environment Observation, Institute of Atmospheric Physics, Chinese Academy of Sciences, Beijing 100029, China*

⁵ *Key Laboratory for Semi-Arid Climate Change of the Ministry of Education, College of Atmospheric Sciences, Lanzhou University, Lanzhou, China*

⁶ *National Observation and Research Station for Qomolangma Special Atmospheric Processes and Environmental Changes, Dingri 858200, China*

Corresponding authors: Yilong Wang (wangyilong@itpcas.ac.cn) and Minzheng Duan (dmz@mail.iap.ac.cn)

Abstract

The Qinghai-Tibetan Plateau (QTP) is a key system that impacts the global carbon balance, but greenhouse gases (GHGs) mole fraction measurements in this region are limited due to the tough environment. Supported by the Second Tibetan Plateau Scientific Expedition Program, we carried out an integrated GHG measurement campaign in May 2022 as part of the Earth Summit Mission-2022 at the Qomolangma station for atmospheric and environmental observation and research (QOMS; 28.362°N, 86.949°E, 4276 m a.s.l.). In this study, the first GHG column-averaged mole fraction measurements (X_{gas}) at QOMS are presented, including XCO₂, XCH₄, XCO, and XN₂O, derived from a ground-based Fourier-transform infrared spectrometer (FTIR; Bruker EM27/SUN). We then compare them to surface *in situ* and satellite (TROPOMI and OCO-2) measurements. The



mean FTIR XCO₂ and XCH₄ are 7.8 ppm and 97 ppb less than those near the surface, respectively. The difference between OCO-2 land nadir and EM27/SUN XCO₂ measurements is 0.21 ± 0.98 ppm, which is consistent with OCO-2 retrieval uncertainty. However, a relatively large bias (1.21 ± 1.29 ppm) is found for OCO-2 glint XCO₂ measurements, which is related to the surface albedos and surface altitudes. The EM27/SUN measurements indicate that the uncertainty of OCO-2 satellite XCO₂ measurements is relatively large in the QTP mountain region and its quality needs to be further assessed. The difference between FTIR and TROPOMI XCO measurements is -5.06 ± 5.36 (1σ) ppb ($-4.7 \pm 5.1\%$) within the satellite retrieval uncertainty. The XCO measurements at QOMS show the local air mass is largely influenced by atmospheric transport from southern Asia, and it is important to carry out long-term measurements to quantify the contribution of the cross-regional transport in this region.

Keywords: Qomolangma, greenhouse gas, EM27/SUN, OCO-2, TROPOMI

1 Introduction

The Qinghai-Tibetan Plateau (QTP) plays an important role in regional and global climate systems (Ge et al. 2017; Tada et al. 2016; Zhang et al. 2021). The high mountains in the QTP, including the Earth's highest summit (Mt. Qomolangma; 8848.86 m a.s.l.), strongly affect the atmospheric thermodynamic and dynamic conditions. On the other hand, environmental changes, including human activities, atmospheric warming, and cryosphere thaw, can in turn make significant impacts on the hydrology, ecosystems, and biogeochemistry in the QTP (Rui et al. 2011; Wu et al. 2021; Zhang et al. 2015). The QTP has abundant original forest and soil resources, and serves as a huge carbon storage (Ding et al. 2016; Wang et al. 2020; Jia et al. 2021). A small change in carbon storage of the QTP could make an impact on the global carbon balance. However, there is still a large uncertainty about the terrestrial ecosystem carbon sink in the QTP (Wang et al. 2021; Piao et al. 2022). The uncertainties associated with eddy covariance data processing may lead to an overestimation of the carbon sink (Wang et al. 2022). Using a 'top-down' approach can help us to estimate the carbon sink in the QTP (Jiang et al. 2016). However, limited greenhouse gases (GHGs) measurements are currently available in this region because of the tough environment (Guo et al. 2020; Liu et al. 2021; Zhou et al. 2023).



62 To better understand the level and temporal variation of atmospheric GHGs mole fraction over
63 the QTP, we carried out an integrated GHGs measurement campaign at the Qomolangma station
64 for atmospheric and environmental observation and research, Chinese Academy of Sciences
65 (QOMS) in May 2022 as part of the Second Tibetan Plateau Scientific Expedition Program (Earth
66 Summit Mission-2022). During this campaign, a compact Fourier-transform infrared spectrometer
67 (FTIR), Bruker EM27/SUN, was applied to retrieve the column-averaged dry air mole fraction of
68 CO₂, CH₄, CO, and N₂O (XCO₂, XCH₄, XCO, and XN₂O) at QOMS between 5 and 24 May 2022.
69 The FTIR measures the GHG columns, which are less affected by the local meteorological
70 parameters, such as the boundary layer height and wind turbulence (Wunch et al. 2011; Zhou et
71 al. 2018). The ground-based FTIR GHGs measurement is widely used to validate satellite
72 observation because of its high precision and similar measurement technique to the satellite (Zhou
73 et al. 2016; Wunch et al. 2017; Sha et al. 2021). In addition, a gas analyzer (ABB Ultra-Portable
74 Greenhouse Gas Analyzer; GLA132), using a the off-axis integrated cavity output spectroscopy
75 (OA-ICOS) technique, was applied to measure the CO₂ and CH₄ mole fractions near the surface.
76 In the following sections, we will give an introduction to the observation site, and present the
77 XCO₂, XCH₄, XCO, and XN₂O derived from the EM27/SUN FTIR spectra at QOMS. The results
78 from the *in situ* and ground-based FTIR measurements are shown in Section 3. In Section 4, the *in*
79 *situ* surface measurements are compared to the FTIR column measurements. Moreover, the FTIR
80 measurements are then compared to independent satellite observations. Finally, the conclusions
81 are drawn in Section 5.

82 2 Observation site and data

83 2.1 The QOMS site

84 The QOMS (latitude 28.362°N; longitude 86.949°E; with an elevation of 4276 m a.s.l.) is
85 situated approximately 30 km away from the Everest Base Camp and around 650 km from Lhasa
86 (Figure 1). The station is located about 3 km to the south of the local village, in an area with
87 minimal human influence. The surface of the station is flat, and it is mainly covered by sand and
88 gravel with sparse vegetation. More information about the QOMS refers to Ma et al. (2023).

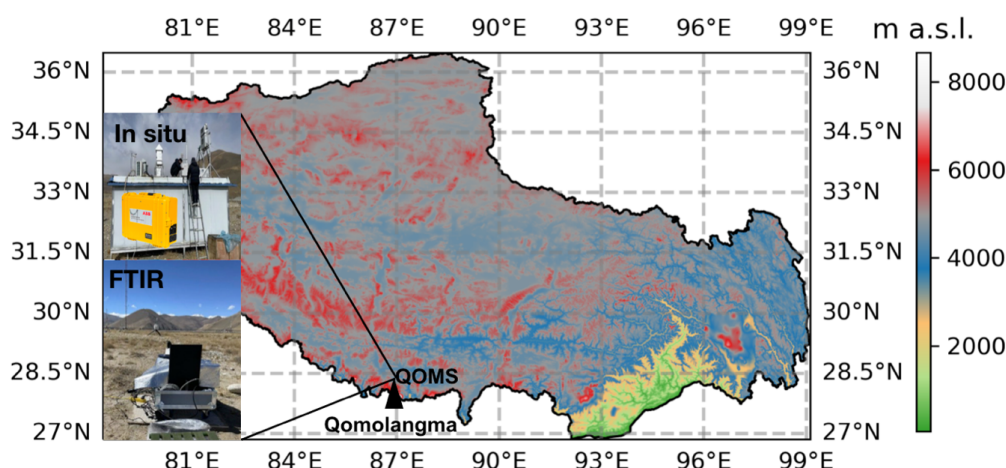


Figure 1. The integrated GHGs measurement campaign carried out at the Qomolangma station for atmospheric and environmental observation and research station (QOMS) in May 2022 including both the FTIR remote sensing and surface *in situ* measurements.

2.2 Ground-based FTIR

A Bruker EM27/SUN FTIR was operated at QOMS between 5 and 24 May. The measurement settings of the EM27/SUN follow the guidance of the Collaborative Carbon Column Observing Network (COCCON), which records the direct solar absorption spectra between 4000 and 12000 cm^{-1} with a spectral resolution of 0.5 cm^{-1} using two InGaAs detectors (Frey et al., 2019). The advanced retrieval algorithm GGG2020 is applied to retrieve the O_2 and GHGs (CO_2 , CH_4 , CO , and N_2O) total columns, and then X_{gas} is calculated as $0.2095 (TC_{\text{GHG}}/TC_{\text{O}_2})$. Using the ratio between target species and O_2 can reduce the same uncertainty from the instrumental and atmospheric parameters (Yang et al. 2002). GGG2020 is commonly used in the ground-based GHG remote sensing community, and it includes: 1) the conversion from interferogram to spectrum with the DC correction (Keppel-Aleks et al. 2012); 2) a non-linear least squares fitting code (GFIT); 3) a post-correction procedure to reduce the retrieval uncertainty resulting from spectroscopy and observation geometry (Laughner et al. 2023). To further reduce the systematic uncertainty of the EM27/SUN retrievals, the EM27/SUN instrument was operated together with the TCCON site at Xianghe (Yang et al. 2020) for three weeks in July-August 2022 after the campaign. Based on the co-located measurements of EM27/SUN and TCCON, the scaling factors



110 of 1.001, 0.995, 0.970, and 1.004 have been derived and applied to correct the systematic
111 uncertainties of the EM27/SUN XCO₂, XCH₄, XCO, and XN₂O retrievals, respectively.

112 2.3 *In situ*

113 The near-surface CO₂ and CH₄ mole fractions were observed by the ABB GLA132 gas
114 analyzer at QOMS continuously between 13 and 24 May 2022 (Figure 1). To ensure the accuracy
115 of the GHG *in situ* measurements, we calibrated the gas analyzer using the standard gas once per
116 day. The precisions of the *in situ* measurements (1 second) are within 0.3 ppm and 2.0 ppb for CO₂
117 and CH₄, respectively ([https://www.envicontrol.com/storage/app/media/uploaded-](https://www.envicontrol.com/storage/app/media/uploaded-files/UGGA%20LGR%20GLA132-GGA.pdf)
118 [files/UGGA%20LGR%20GLA132-GGA.pdf](https://www.envicontrol.com/storage/app/media/uploaded-files/UGGA%20LGR%20GLA132-GGA.pdf)). Note that the drifts of CO₂ and CH₄ within 24
119 hours of the analyzer are within their measurement uncertainties.

120 2.4 *Satellite*

121 We use the Orbiting Carbon Observatory-2 (OCO-2) satellite level 2 bias-corrected XCO₂
122 retrospective processing v11.2r (Kiel et al. 2019). The OCO-2 XCO₂ is retrieved using the ACOS
123 algorithm by the CO₂ absorption lines around 1.61 and 2.06 μm, together with the information
124 about surface pressure, cloud and aerosol scattering constrained by the O₂-A band around 0.76 μm
125 (O'dell et al. 2018). For more details about the OCO-2 XCO₂ data, we refer to the
126 https://docserver.gesdisc.eosdis.nasa.gov/public/project/OCO/OCO_L2_ATBD.pdf. The OCO-2
127 XCO₂ uncertainty has been accessed by comparing to the Total Carbon Column Observing
128 Network (TCCON), and the absolute median difference across TCCON sites over the globe is
129 found to be less than 0.4 ppm and the root mean square of the differences is less than 1.5 ppm
130 (Wunch et al. 2017). The footprint size of each OCO-2 pixel is 2.25×1.29 km². However, the width
131 of the swath is only about 16 km, leading to a very small spatial coverage. During the campaign,
132 there were 2 days when the orbit of OCO-2 overpassed within 500 km around QOMS. These OCO-
133 2 satellite measurements are compared to EM27/SUN FTIR measurements to assess their quality
134 at QOMS.

135 Regarding CH₄ and CO, we use the ESA operational offline level 2 products from the Sentinel-
136 5 Precursor (S5-P) TROPOspheric Monitoring Instrument (TROPOMI). Unfortunately, there is
137 almost no TROPOMI CH₄ retrieval at QOMS, mainly due to the complex orography and high
138 cloud coverage in this region (Lorente et al. 2021). Therefore, in this study, we only look at the
139 TROPOMI XCO data. The TROPOMI XCO retrievals are derived from the reflected solar
140 radiation in 2.3 μm band and the stripes of erroneous XCO retrievals are corrected by the fixed



masked de-stripping method (Landgraf et al. 2016; Borsdorff et al. 2019). The spatial resolution of TROPOMI measurements is $7.0 \times 5.5 \text{ km}^2$. Thanks to the large swath of about 2600 km, TROPOMI provides XCO measurements in this region around 15:30 China Standard Time (CST) every day. According to the validation study made by Martínez-Alonso et al. (2022), the mean difference between TROPOMI XCO data and AirCore measurements is $2.02 \pm 11.13 (1\sigma) \%$.

3 Results

3.1 Ground-based FTIR column measurements

The time series together of *a priori* and retrieved XCO_2 , XCH_4 , XCO, and XN_2O measurements from the EM27/SUN FTIR at QOMS between 5 and 24 May are shown in Figure 2. The *a priori* columns of FTIR retrievals are derived from the global atmospheric chemistry model (GEOS-FPIT), which provides 6-hourly simulations with a spatial resolution of about 50 km. For more information about the GGG2020 *a priori* profiles, please refer to Laughner et al. (2023). Keep in mind that the FTIR provides the measurements only in the daytime and under a clear sky condition.

The mean and std of XCO_2 , XCH_4 , XCO, and XN_2O are $418.4 \pm 0.6 \text{ ppm}$, $1888.3 \pm 8.0 \text{ ppb}$, $106.2 \pm 8.3 \text{ ppb}$, and $321.6 \pm 3.2 \text{ ppb}$, respectively. The EM27/SUN retrieved columns are larger than the *a priori* columns (GEOS-PFIT model simulations) for all these four species, indicating that the model is systematically underestimated in this region. In addition, the amplitudes of the variations of XCO_2 and XCH_4 derived from the EM27/SUN measurements are larger than the model simulations. Moreover, the day-to-day variations of these species are not well captured by the GEOS-PFIT model, for example, the maximum XCO value observed by the FTIR measurements on 16 May is not well-simulated in the model. The mean of XCO_2 , XCH_4 , and XCO observed at QOMS are also compared to six TCCON sites (Hase et al. 2023; Té et al. 2022; Warneke et al. 2022; Wennberg et al. 2022a,b; Zhou et al. 2022) in the mid-latitude northern hemisphere during the same time period (Table 1). The mean XCO_2 at QOMS is lowest among these sites, which is about 1.5–3.5 ppm less than urban sites, and about 0.5–1.5 ppm less than suburban sites. The XCH_4 and XCO observed at QOMS are less than those at Xianghe and Caltech, but larger than other TCCON sites.

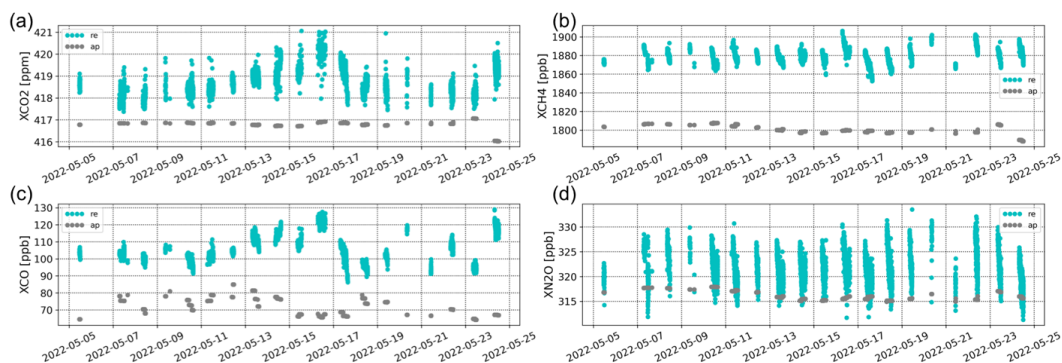
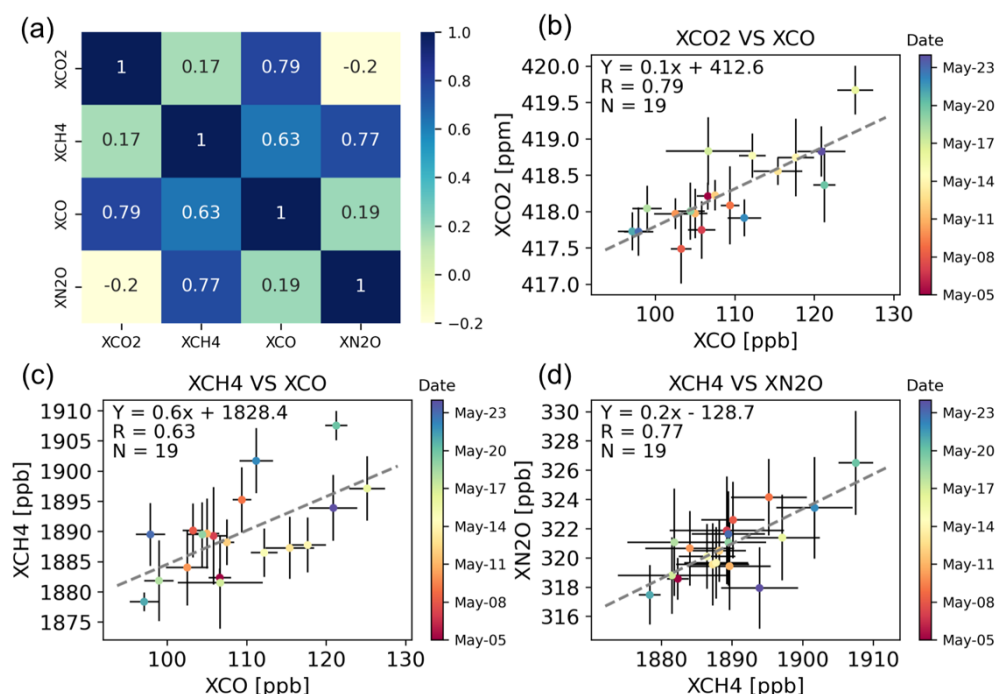


Figure 2. The time series of *a priori* (grey dots) and retrieved (cyan dots) XCO₂, XCH₄, XCO, and XN₂O measurements from the EM27/SUN FTIR between 5 and 24 May 2022 at QOMS.

Table 1. The mean and std of the XCO₂, XCH₄, XCO measurements at six mid-latitude TCCON sites in the northern hemisphere, together with our EM27/SUN measurements at QOMS. N is the number of measurements at each site between 5 and 24 May 2022.

Type	Site	Geolocation	XCO ₂ (ppm)	XCH ₄ (ppb)	XCO (ppb)	N
Urban	Paris	48.84°N;2.35°E;60 m	420.1±0.9	1870.4±4.2	97.9±7.2	685
	Xianghe	39.8°N;116.96°E;36 m	419.9±0.8	1906.7±12.1	134.4±15.3	268
	Caltech	34.13°N;118.12°W;230m	421.9±0.9	1899.2±6.8	117.6±6.4	1956
Suburb	Karlsruhe	49.1°N;8.439°E;116 m	418.9±0.8	1876.3±9.2	99.2±3.9	533
	Orleans	47.97°N;2.113°E;130m	418.9±0.8	1875.9±7.5	96.2±5.9	1641
	Lamont	36.6°N;97.486°W;320 m	419.9±0.7	1885.6±6.1	105.1±7.8	838
QTP	QOMS	28.3°N; 86.9°E; 4276 m	418.4±0.6	1888.3±8.0	106.2±8.3	5925

Figure 3 shows the covariance matrix among these four species observed by the EM27/SUN measurements. The good correlations are found between XCO₂ and XCO ($R=0.79$; $p_value<0.001$), XCH₄ and XCO ($R=0.63$; $p_value<0.01$), XCH₄ and XN₂O ($R=0.77$; $p_value<0.001$). However, the correlations are relatively weak between XCO₂ and XCH₄ ($R=0.16$; $p_value=0.50$), XCO₂ and XN₂O ($R=-0.20$; $p_value=0.41$), XCO and XN₂O ($R=0.19$; $p_value=0.43$). The good correlation between XCH₄ and XN₂O is probably due to their similar physical and chemical process in the stratosphere (Wang et al. 2014; Ji et al. 2020).



186

187 **Figure 3.** The correlation matrix among XCO₂, XCH₄, XCO and XN₂O observed by the
 188 EM27/SUN measurements between 5 and 24 May 2022 at QOMS (a), together with the scatter
 189 plots between XCO₂ and XCO daily means (b), between XCH₄ and XCO daily means (c), and
 190 XCH₄ and XN₂O daily means (d). In each scatter plot, the error bar denotes the daily std, the dashed
 191 line is the linear regression, R is the Pearson correlation coefficient, and N is the number of the
 192 co-located measurements. The dot is colored by the measurement date.

193

194 The EM27/SUN measurements indicate that XCO is a good tracer for both XCO₂ and
 195 XCH₄ at QOMS, while the R between XCO₂ and CH₄ is only 0.17. To better understand this, we
 196 separate the time period into 3 weeks (Table 2). The R values are relatively low in the first week,
 197 especially between XCO₂ and XCH₄. The day-to-day variations of these species are pretty low in
 198 the first week (Figure 2). In the second week, large enhancements of the three species on 16 May
 199 are observed simultaneously, resulting in large R values. In the third week, strong vibrations in
 200 XCO₂, XCH₄, and XCO are observed, but unlike a single large enhancement in the second week,
 201 the enhancements in this week are discontinuous. The R values in the third week are larger than
 202 those in the first week, but less than those in the second week. Based on the three weeks, we
 203 understand that a good correlation (R=0.83) between XCO₂ and XCH₄ can be also observed when



204 a large continuous enhancement occurs. However, the correlation between XCO_2 and XCH_4
 205 becomes low and even negative ($R=-0.26$), when the variations of XCO_2 and XCH_4 are low.

206

207 **Table 2.** The correlations among XCO_2 , XCH_4 , and XCO in the first week (5-11 May), second
 208 week (12-18 May), and third week (19-24 May).

R	XCO_2 and XCH_4	XCO_2 and XCO	XCH_4 and XCO
Week 1 (5-11 May)	-0.26	0.60	0.46
Week 2 (12-18 May)	0.83	0.91	0.84
Week 3 (19-24 May)	0.40	0.89	0.79

209

210 *3.2 In situ CO_2 and CH_4 measurements near the surface*

211 The time series of CO_2 and CH_4 observed by the gas analyzer at QOMS near the surface
 212 between 13 and 24 May, together with their diurnal variations, are shown in Figure 4. The mean
 213 and std of CO_2 and CH_4 are 424.2 ± 2.1 ppm and 1985.2 ± 19.7 ppb, respectively. A good correlation
 214 between CO_2 and CH_4 is observed, with a Pearson correlation coefficient (R) of 0.82. Similar to
 215 the FTIR XCO_2 and XCH_4 , the surface CO_2 and CH_4 mole fractions are the highest on 16 May.
 216 The mean CO_2 mole fraction in the daytime is about 0.9 ppm higher than that during the night.
 217 Contrary to CO_2 , we observe the minimum CH_4 value at around 13:00, which is about 12 ppb less
 218 than that at midnight.

219

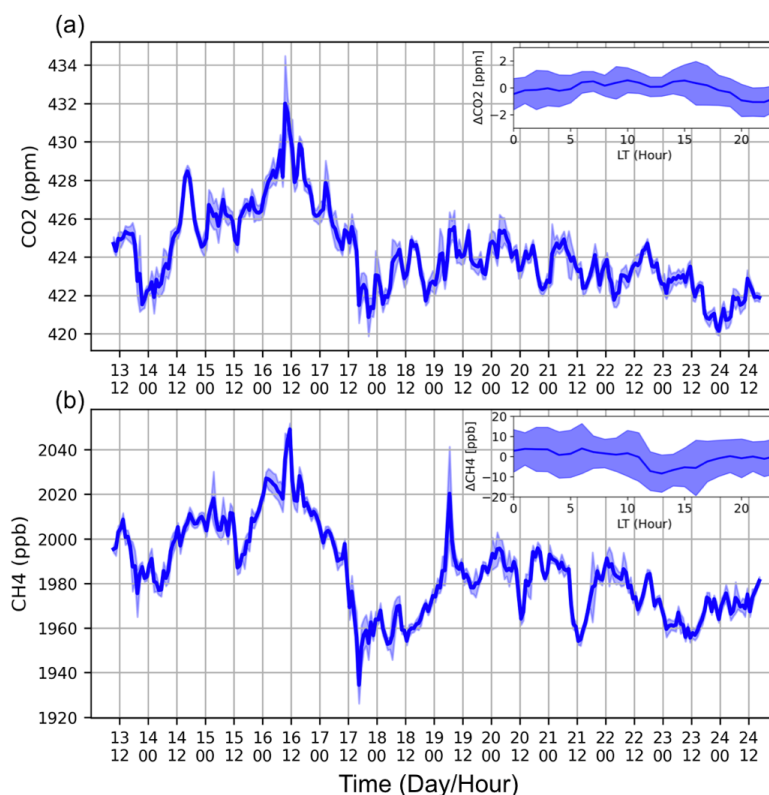


Figure 4. The time series of hourly mean and std of CO₂ (a) and CH₄ (b) mole fraction observed by the gas analyzer at QOMS near the surface. The small panel in the right-upper corner shows the daily variation of CO₂ and CH₄.

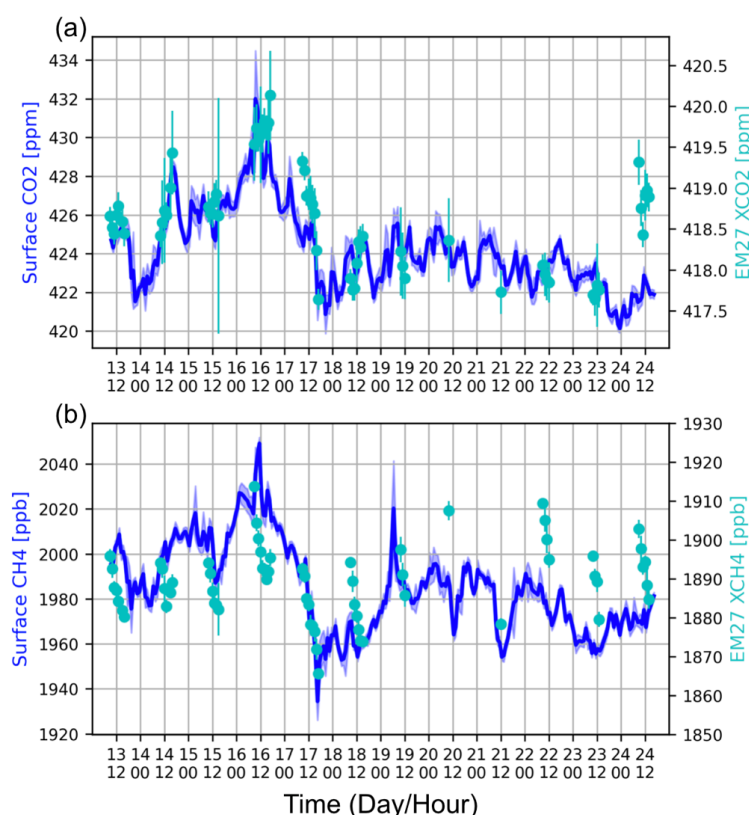
4 Inter-comparisons and discussions

4.1 Comparison between FTIR column and surface *in situ* measurements

The FTIR observes the CO₂ and CH₄ columns, while the *in situ* provides the surface mole fractions. Do the variations of XCO₂ and XCH₄ differ from the surface measurements? Here, CO₂ and CH₄ surface mole fractions are compared with the FTIR XCO₂ and XCH₄ measurements (Figure 7). The mean CO₂ surface mole fraction is 7.8 ppm larger than the XCO₂, and the mean CH₄ surface mole fraction is 97 ppb larger than the XCH₄. The amplitude of the variation of CO₂ surface variation during this period is 4.8 times larger than the amplitude of the variation of XCO₂. The CH₄ mole fractions in the stratosphere are much lower than those in the troposphere due to the chemical reaction and atmospheric dynamic transport (Sepúlveda et al. 2014; Wang et al. 2014). According to the GEOS-PFIT model, CO₂ mole fraction also decreases with altitude, especially



235 above the tropopause height (Laughner et al. 2023). A good correlation between the surface CO₂
236 and XCO₂ is found, with an R of 0.74 (p_value<0.001). The CO₂ enhancement on 16 May was
237 observed both near the surface and in the column. We also notice that relatively high XCO₂ was
238 observed on 24 May but with low CO₂ mole fractions at the surface. It is indicated that CO₂
239 enhancement occurs at high altitudes but not at the surface.



240

241 **Figure 5.** Similar to Figure 4, but adding the EM27/SUN FTIR XCO₂ and XCH₄ hourly means
242 and stds between 13 and 24 May 2022.
243

244 Similar to CO₂, the amplitude of the variation of CH₄ near the surface during this period is
245 2.9 times larger than the amplitude of the variation of XCH₄. The correlation between the surface
246 CH₄ and XCH₄ is relatively weak as compared to that between CO₂ and XCO₂ but still statistically
247 significant (R=0.41; p_value<0.01). The weak correlation in CH₄ is probably due to that CH₄ has
248 a much larger vertical gradient than the CO₂ between the troposphere and the stratosphere
249 (Sepúlveda et al. 2014). Therefore, vertical transport in the upper troposphere and lower

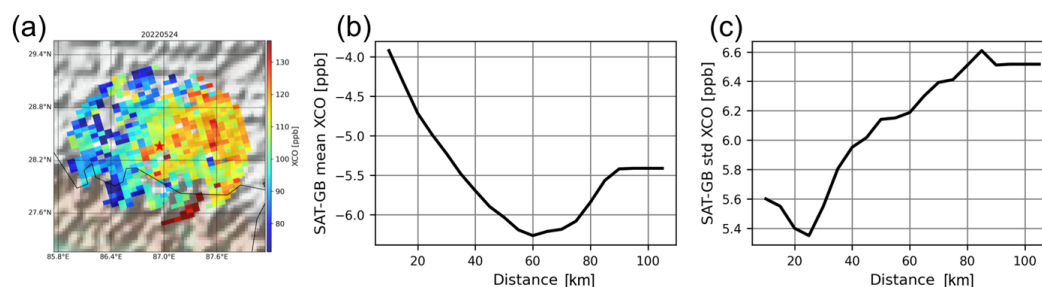


250 stratosphere (UTLS) and horizontal transport in the stratosphere both make strong impacts on CH₄
251 column. Nevertheless, the CH₄ enhancement on 16 May was observed both near the surface and
252 in the column.

253

254 4.2 Ground-based FTIR against TROPOMI XCO measurements

255 In this section, we compare the ground-based EM27/SUN FTIR measurements (GB) to the
256 TROPOMI satellite XCO measurements (SAT) at QOMS. We use the mean of GB measurements
257 within ± 2 hours of each satellite overpass time (approximately from 12:30 to 17:30 LT), and select
258 all the satellite measurements within a certain distance around QOMS. For each SAT-GB data pair,
259 we apply the SAT *a priori* profile (TM5 model) as the common prior to reducing the uncertainty
260 from different *a priori* profiles (Rodgers and Connor 2003). In addition, to get rid of the
261 discrepancy caused by different surface altitudes of the FTIR and satellite measurements, the FTIR
262 retrieved XCO is scaled to the same vertical range of each satellite measurement (Langerock et al.
263 2015). Figures 6b and 6c show the mean and std of the differences between co-located TROPOMI
264 satellite and ground-based FTIR XCO measurements (SAT-GB) between 5 and 24 May, varying
265 with the co-located distance criterion ranging from 10 to 105 km. The mean difference varies
266 between -3.9 and -6.3 ppb. The mean difference enlarges with increasing distance between FTIR
267 and TROPOMI measurements, while the std reaches the minimum (5.36 ppb) at the distance of 25
268 km. To ensure enough data pairs to get a robust comparison, we set the co-located distance to 25
269 km, resulting in 17 days with co-located FTIR and satellite measurements.



270

271 **Figure 6.** The TROPOMI XCO measurements within 100 km around the QOMS (red star) on 24
272 May 2022 (a). The mean (b) and std (c) of the differences between co-located TROPOMI satellite
273 and ground-based EM27/SUN XCO measurements (SAT-GB) between 5 and 24 May varying with
274 the co-located distance criterion.

275



The time series and scatter plot of the co-located FTIR and TROPOMI satellite XCO measurements at QOMS are shown in Figure 7. A good correlation between FTIR and TROPOMI XCO measurements is observed, with the R value of 0.81 ($p_value < 0.001$). The difference between FTIR and TROPOMI XCO measurements is -5.06 ± 5.36 ppb ($-4.7 \pm 5.1\%$), which is within the S5P mission requirements with a systematic error of 15% and random error of 10%. The relative bias at QOMS is also comparable with other places around the world (Sha et al. 2021; Martínez-Alonso et al. 2022). The EM27/SUN measurements at QOMS thus indicate that the TROPOMI XCO data has a good performance in this region.

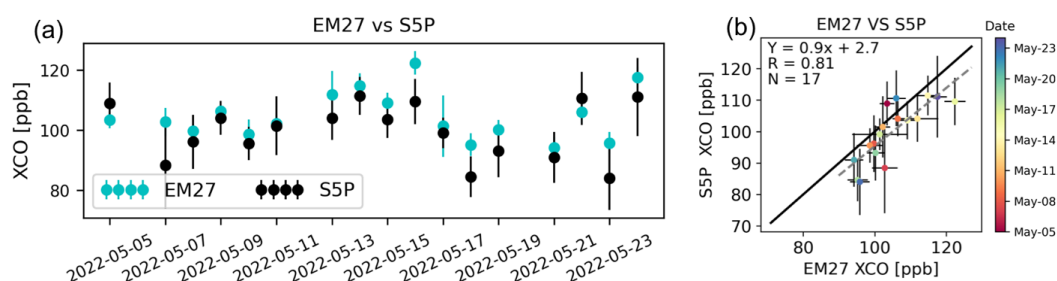


Figure 7. The co-located TROPOMI/S5P and EM27/SUN XCO measurements between 5 and 24 May 2022 (a). The errorbar of the satellite measurement is the std of all measurements within 25 km around the site, and the errorbar of the FTIR measurement is the std of all measurements within ± 2 hours within the satellite overpass time. The scatter plot of the TROPOMI/S5P and EM27/SUN XCO co-located measurements (b). The dashed line is the linear regression, R is the Pearson correlation coefficient, and N is the number of the co-located measurements. The dot is colored by the measurement date.

The high and low XCO values at QOMS are observed simultaneously from the ground-based FTIR and TROPOMI satellite measurements. Thanks to the good coverage of the TROPOMI satellite measurements, it is applied to show the spatial distributions of XCO around QOMS in a larger domain. Figure 8 shows the TROPOMI XCO measurements on 16, 22, and 24 May with relatively high XCO values, and on 18, 21, and 23 May, with relatively low XCO values around QOMS. The wind speed and wind direction are derived from the ERA5 reanalysis pressure-level data at 500 hPa (~ 5 km a.s.l.). We find that XCO at the south side of Mt. Qomolangma is much larger than that at the side edge, because of high anthropogenic emissions in Nepal and India (Crippa et al. 2018). The relatively high XCO values at QOMS on 16, 22, and 24 May correspond to south winds, which bring the air mass with high CO mole fraction to QOMS. On 18 and 21 May,



the wind direction was from the west to the east along the southern edge of the Himalayas mountains and did not bring air mass to QOMS so low XCO values are observed in all regions of the southern Tibetan Plateau. On 23 May, relatively high XCO values are observed at approximately 200 km west or east of QOMS, but low XCO values are observed at QOMS. Based on the TROPOMI satellite measurements and the wind data, we conclude that the day-to-day variation of XCO observed at QOMS is largely influenced by atmospheric transport, and the air mass transported from southern Asia can enhance the CO mole fractions over the Tibetan Plateau.

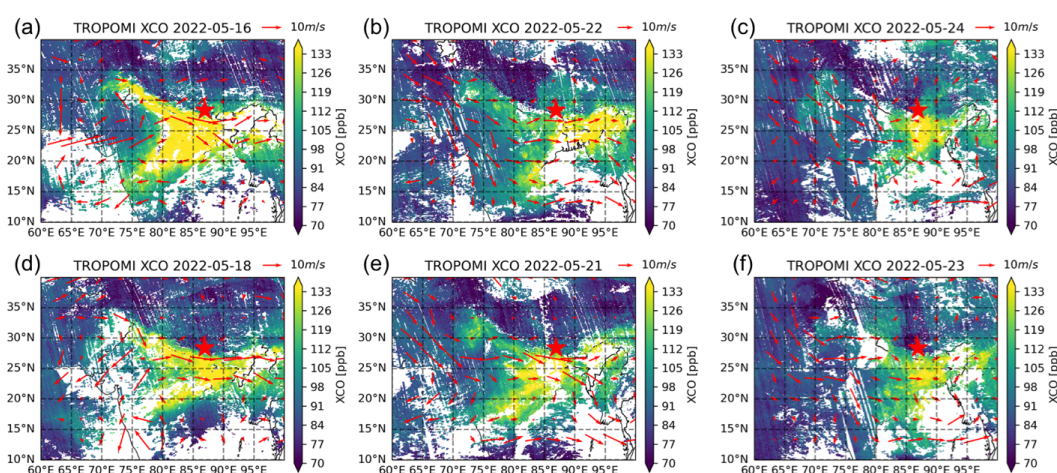


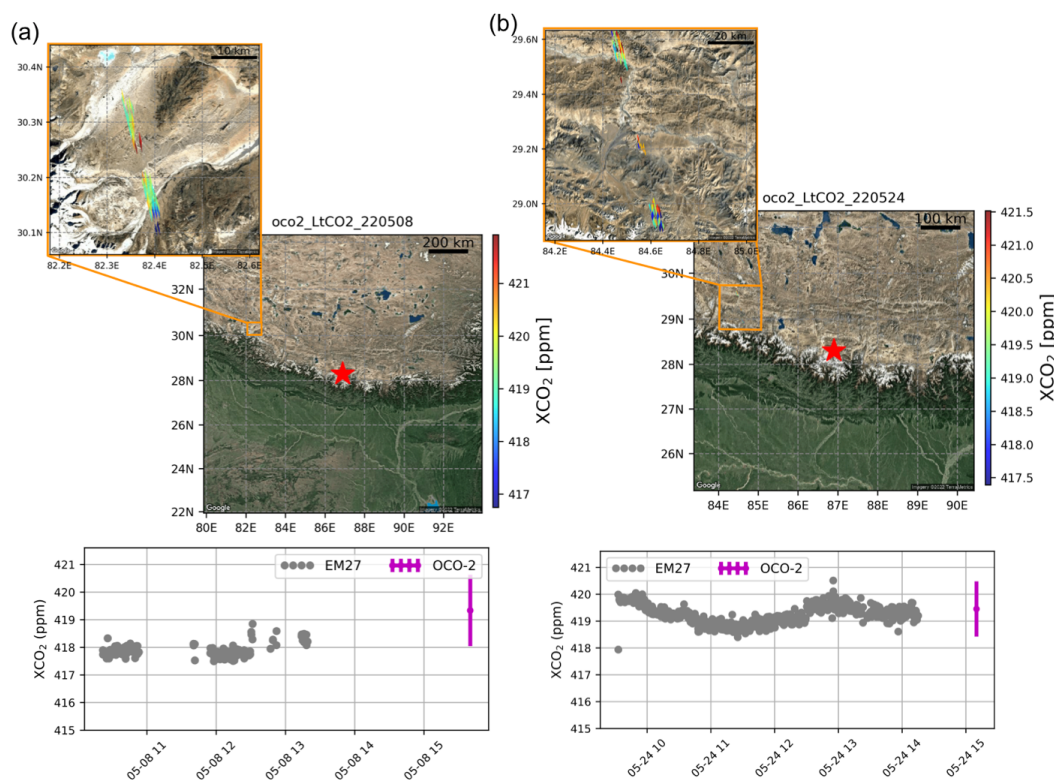
Figure 8. The XCO₂ observed by the TROPOMI/S5P satellite on 16 (a), 22 (b), and 25 (c) May 2022, with relatively high XCO₂ values at QOMS (remarked as the red star), and on 18 (d), 21 (e), and 23 (f) May 2022, with relatively low XCO₂ values at QOMS. The wind direction and wind speed are derived from the ERA5 reanalysis data at 500 hPa (~ 5 km a.s.l.).

4.3 Ground-based FTIR against OCO-2 XCO₂ measurements

Unlike the TROPOMI XCO₂ measurements, very limited OCO-2 XCO₂ measurements are available due to its narrow swath. During this campaign, we only had two days, when the OCO-2 satellite provided valid measurements (qflag = 0) around QOMS (Figure 9). The distances between the OCO-2 measurements and the FTIR site are about 480 km and 250 km on 8 and 24 May, respectively. Note that the observation mode of OCO-2 is land glint on 8 May and land nadir on 24 May. As the OCO-2 and EM27/SUN both use GEOS-FPIT model simulations as the *a priori* profiles, no prior substitution correction is needed (Zhou et al. 2016). For each FTIR-satellite data pair, we correct the FTIR measurement to the same altitude of the satellite footprint. As we do not



328 have the FTIR measurement around the OCO-3 overpass time (~15:30 CST), we use the mean of
329 the FTIR measurements in the latest 1 hour.
330

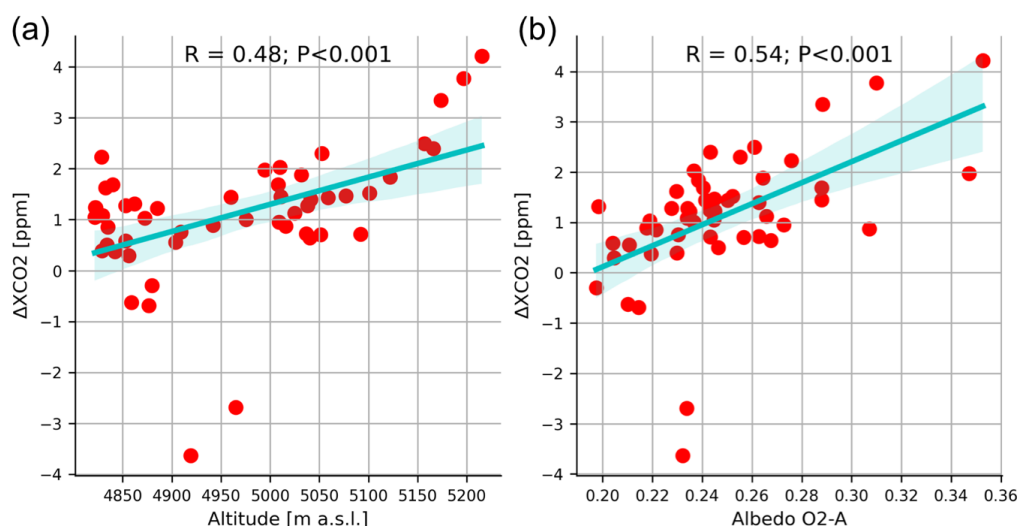


331
332 **Figure 9.** The XCO₂ observed by the OCO-2 satellite with glint mode on 8 May (a) and with nadir
333 mode on 24 May (b) around QOMS (remarked as the red star on the satellite image from © Google
334 Maps). For each day, the time series of the EM27/SUN XCO₂ individual measurements are shown
335 together with the mean and std of all co-located OCO-2 measurements in the bottom panels.
336

337 The mean and std of the differences between EM27/SUN and OCO-2 XCO₂ measurements
338 (SAT-GB) are 1.21 ± 1.29 ppm and 0.21 ± 0.98 ppm on 8 and 24 May, respectively. The bias of
339 OCO-2 XCO₂ measurements at QOMS is in the same order of magnitude as the bias found at
340 global TCCON sites (Wunch et al. 2017). The reported uncertainty of the OCO-2 XCO₂ nadir
341 measurements on 24 May is 0.65 ppm, which is slightly lower than the std of 0.98 ppm. However,
342 the reported uncertainty of the OCO-2 XCO₂ glint measurements on 8 May is 0.57 ppm, which is
343 much smaller than the std of 1.29 ppm.



344 The OCO-2 measurements on these two days are both concentrated in a small region
345 without intense human activity. It is assumed that the XCO_2 is stable in such a region. Figure 10
346 shows the bias of OCO-2 glint measurements (SAT-GB) varying with surface altitudes and
347 retrieved surface albedos in the O_2 -A band on 8 May 2022. It is found that the bias of OCO-2 land
348 glint measurements is strongly related to the retrieved surface albedos ($R=0.54$) and footprint
349 surface altitudes ($R=0.48$). Further correction of OCO-2 glint measurements in this region using
350 the O_2 -A band surface albedo/surface altitude is recommended, but more data are required.
351 Regarding the OCO-2 land nadir measurements on 24 May, we do not find significant correlations
352 between the bias and altitudes ($R=-0.26$) or surface albedos ($R=0.17$). Instead, the biases are
353 randomly distributed.



354
355 **Figure 10.** The bias of XCO_2 observed by OCO-2 land glint measurements ($\Delta XCO_2 = SAT-GB$)
356 on 8 May 2022 varying with surface altitude (a) and surface albedo in O_2 -A band (b).

357 5 Conclusions

358 The QTP serves as a huge carbon storage but is also sensitive to climate change. Currently,
359 there is still a large uncertainty about the terrestrial ecosystem carbon sink in the QTP. Due to the
360 tough environment, GHG measurements are scarce. In May 2022, an integrated greenhouse gases
361 measurement campaign was carried out at QOMS within the framework of the Second Tibetan
362 Plateau Scientific Expedition Program. In this study, we present the experiments about the *in situ*



363 measurements near the surface and the ground-based EM27/SUN FTIR column measurements.

364 The following results are presented and discussed:

- 365 1) The *in situ* measurements near the surface at QOMS between 13 and 24 May 2022 show
366 that the CO₂ and CH₄ mole fractions are 424.2±2.1 ppm and 1985.2±19.7 ppb, respectively.
367 In addition, a good correlation (R=0.82) between the surface CO₂ and CH₄ mole fractions
368 is observed.
- 369 2) The ground-based FTIR measurements at QOMS between 5 and 24 May show that the
370 mean XCO₂, XCH₄, XCO, and XN₂O are 418.4±0.6 ppm, 1888.3±8.0 ppb, 106.2±8.3 ppb,
371 and 321.6±3.2 ppb, respectively. The mean of XCO₂ at QOMS is about 0.5-3.5 ppm lower
372 than six TCCON sites in the mid-latitude northern hemisphere during the same time period.
373 The GHG measurements at QOMS seriously differ from the GEOS-PFIT model
374 simulations, indicating the large uncertainty of the model simulations in this region.
- 375 3) The ground-based FTIR measurements at QOMS are compared to TROPOMI XCO
376 satellite observations. The difference between FTIR and TROPOMI XCO measurements
377 is -5.06±5.36 ppb (-4.7±5.1%), which is within the S5P mission requirements. A good
378 correlation between FTIR and TROPOMI XCO measurements is also found, with an R of
379 0.81. Utilizing the good spatial coverage of TROPOMI satellite measurements together
380 with the wind data, we find that the day-to-day variation of XCO observed at QOMS is
381 largely affected by atmospheric transport. It is important to carry out long-term
382 measurements to calculate the cross-regional transport in this region quantitatively.
- 383 4) The ground-based FTIR measurements at QOMS are also compared to OCO-2 XCO₂
384 observations. There were only two days with OCO-2 measurements within 500 km around
385 QOMS (land glint mode on 8 May 2022 and land nadir mode on 24 May 2022). The mean
386 differences between FTIR and OCO-2 XCO₂ measurements are 1.21±1.29 ppm and
387 0.21±0.98 ppm on 8 and 24 May, respectively. It is found that the bias of OCO-2 glint
388 measurements on 8 May is relatively large, and it is statistically related to the retrieved
389 surface albedos and surface altitudes. The quality of the OCO-2 XCO₂ land glint
390 measurements in this region should be further assessed when more ground-based
391 measurements become available.
- 392



393 Data availability

394 The TCCON data were obtained from the TCCON Data Archive hosted by CaltechDATA at
395 <https://tccodata.org>. The TROPOMI satellite data are available at
396 <https://dataspace.copernicus.eu/> (registration request). OCO-2 satellite data are available at
397 <https://ocov2.jpl.nasa.gov/science/oco-2-data-center/> (registration request). The ground-based
398 FTIR measurements at QOMS are available upon request.
399

400 Competing interests

401 The authors declare that they have no conflict of interest.

402 Acknowledge

403 This study is supported by Second Tibetan Plateau Scientific Expedition Program
404 (2022QZKK0101) and the National Natural Science Foundation of China (42205140). The authors
405 would like to thank all staffs at QOMS for supporting the GHG measurement campaign. The
406 authors want to thank TCCON community, ESA, and NASA for providing the TCCON,
407 TROPOMI and OCO-2 data.
408

409 Author contributions

410 MZ, YW, and MZ design the study. MZ wrote the manuscript with inputs from YW and MZ. XT
411 and JD serve as the project leaders of the campaign. JB set up the EM27/SUN instrument. YM,
412 WM, and ZX provided local support to collect the data. All authors have read and commented the
413 manuscript.
414

415 Reference:

- 416 Borsdorff, T., and Coauthors, 2019: Improving the TROPOMI CO data product: update of the
417 spectroscopic database and destripping of single orbits. *Atmospheric Meas. Tech.*, **12**,
418 5443–5455.
- 419 Crippa, M., and Coauthors, 2018: Gridded emissions of air pollutants for the period 1970–2012
420 within EDGAR v4. 3.2. *Earth Syst Sci Data*, **10**, 1987–2013.
- 421 Ding, J., and Coauthors, 2016: The permafrost carbon inventory on the Tibetan Plateau: a new
422 evaluation using deep sediment cores. *Glob. Change Biol.*, **22**, 2688–2701,
423 <https://doi.org/10.1111/gcb.13257>.
- 424 Ge, F., F. Sielmann, X. Zhu, K. Fraedrich, X. Zhi, T. Peng, and L. Wang, 2017: The link
425 between Tibetan Plateau monsoon and Indian summer precipitation: a linear diagnostic
426 perspective. *Clim. Dyn.*, **49**, 4201–4215, <https://doi.org/10.1007/s00382-017-3585-1>.
- 427 Guo, M., and Coauthors, 2020: Comparison of atmospheric CO₂, CH₄, and CO at two stations in
428 the Tibetan Plateau of China. *Earth Space Sci.*, **7**, e2019EA001051.



- 429 Hase, F., B. Herkommer, J. Groß, T. Blumenstock, M. ä. Kiel, and S. Dohe, 2023: TCCON data
430 from Karlsruhe (DE), Release GGG2020.R1.
431 <https://doi.org/10.14291/tccon.ggg2020.karlsruhe01.R1>.
- 432 Ji, D., and Coauthors, 2020: Deriving temporal and vertical distributions of methane in Xianghe
433 Using ground-based Fourier transform infrared and gas-analyzer measurements. *Adv.*
434 *Atmospheric Sci.*, **37**, 597–607.
- 435 Jia, L., and Coauthors, 2021: Carbon storage of the forest and its spatial pattern in Tibet, China.
436 *J. Mt. Sci.*, **18**, 1748–1761.
- 437 Jiang, F., and Coauthors, 2016: A comprehensive estimate of recent carbon sinks in China using
438 both top-down and bottom-up approaches. *Sci. Rep.*, **6**, 22130.
- 439 Keppel-Aleks, G., and Coauthors, 2012: The imprint of surface fluxes and transport on variations
440 in total column carbon dioxide. *Biogeosciences*, **9**, 875–891.
- 441 Kiel, M., C. W. O'Dell, B. Fisher, A. Eldering, R. Nassar, C. G. MacDonald, and P. O.
442 Wennberg, 2019: How bias correction goes wrong: measurement of X_{CO_2} affected by erroneous surface pressure estimates. *Atmospheric Meas.*
443 *Tech.*, **12**, 2241–2259.
- 445 Landgraf, J., and Coauthors, 2016: Carbon monoxide total column retrievals from TROPOMI
446 shortwave infrared measurements. *Atmospheric Meas. Tech.*, **9**, 4955–4975.
- 447 Langerock, B., M. De Mazière, F. Hendrick, C. Vigouroux, F. Desmet, B. Dils, and S. Niemeijer,
448 2015: Description of algorithms for co-locating and comparing gridded model data with
449 remote-sensing observations. *Geosci. Model Dev.*, **8**, 911–921.
- 450 Laughner, J. L., and Coauthors, 2023: A new algorithm to generate a priori trace gas profiles for
451 the GGG2020 retrieval algorithm. *Atmospheric Meas. Tech.*, **16**, 1121–1146.
- 452 Liu, S., and Coauthors, 2021: Changes of atmospheric CO₂ in the Tibetan Plateau from 1994 to
453 2019. *J. Geophys. Res. Atmospheres*, **126**, e2021JD035299.
- 454 Lorente, A., and Coauthors, 2021: Methane retrieved from TROPOMI: improvement of the data
455 product and validation of the first 2 years of measurements. *Atmospheric Meas. Tech.*, **14**,
456 665–684.
- 457 Ma, Y., and Coauthors, 2023: QOMS: A Comprehensive Observation Station for Climate
458 Change Research on the Top of Earth. *Bull. Am. Meteorol. Soc.*, **104**, E563–E584,
459 <https://doi.org/10.1175/BAMS-D-22-0084.1>.
- 460 Martínez-Alonso, S., M. N. Deeter, B. C. Baier, K. McKain, H. Worden, T. Borsdorff, C.
461 Sweeney, and I. Aben, 2022: Evaluation of MOPITT and TROPOMI carbon monoxide
462 retrievals using AirCore in situ vertical profiles. *Atmospheric Meas. Tech.*, **15**, 4751–
463 4765.



- 464 O'dell, C. W., and Coauthors, 2018: Improved retrievals of carbon dioxide from Orbiting Carbon
465 Observatory-2 with the version 8 ACOS algorithm. *Atmospheric Meas. Tech.*, **11**, 6539–
466 6576.
- 467 Piao, S., Y. He, X. Wang, and F. Chen, 2022: Estimation of China's terrestrial ecosystem carbon
468 sink: Methods, progress and prospects. *Sci. China Earth Sci.*, **65**, 641–651.
- 469 Rodgers, C. D., and B. J. Connor, 2003: Intercomparison of remote sounding instruments. *J.*
470 *Geophys. Res. Atmospheres*, **108**.
- 471 Rui, Y., and Coauthors, 2011: Warming and grazing affect soil labile carbon and nitrogen pools
472 differently in an alpine meadow of the Qinghai–Tibet Plateau in China. *J. Soils*
473 *Sediments*, **11**, 903–914, <https://doi.org/10.1007/s11368-011-0388-6>.
- 474 Sepúlveda, E., and Coauthors, 2014: Tropospheric CH₄ signals as observed by NDACC FTIR at
475 globally distributed sites and comparison to GAW surface in situ measurements.
476 *Atmospheric Meas. Tech.*, **7**, 2337–2360.
- 477 Sha, M. K., and Coauthors, 2021: Validation of methane and carbon monoxide from Sentinel-5
478 Precursor using TCCON and NDACC-IRWG stations. *Atmospheric Meas. Tech.*, **14**,
479 6249–6304.
- 480 Tada, R., H. Zheng, and P. D. Clift, 2016: Evolution and variability of the Asian monsoon and its
481 potential linkage with uplift of the Himalaya and Tibetan Plateau. *Prog. Earth Planet.*
482 *Sci.*, **3**, 4, <https://doi.org/10.1186/s40645-016-0080-y>.
- 483 Té, Y., P. Jeseck, and C. Janssen, 2022: TCCON data from Paris (FR), Release GGG2020.R0.
484 <https://doi.org/10.14291/tccon.ggg2020.paris01.R0>.
- 485 Wang, R., and Coauthors, 2021: Monthly Patterns of Ammonia Over the Contiguous United
486 States at 2-km Resolution. *Geophys. Res. Lett.*, **48**,
487 <https://doi.org/10.1029/2020GL090579>.
- 488 Wang, T., D. Yang, Y. Yang, S. Piao, X. Li, G. Cheng, and B. Fu, 2020: Permafrost thawing
489 puts the frozen carbon at risk over the Tibetan Plateau. *Sci. Adv.*, **6**, eaaz3513,
490 <https://doi.org/10.1126/sciadv.aaz3513>.
- 491 Wang, Y., Z. Ding, and Y. Ma, 2022: Data processing uncertainties may lead to an
492 overestimation of the land carbon sink of the Tibetan Plateau. *Proc. Natl. Acad. Sci.*, **119**,
493 e2202343119.
- 494 Wang, Z., and Coauthors, 2014: Retrieval of tropospheric column-averaged CH₄ mole fraction
495 by solar absorption FTIR-spectrometry using N₂O as a proxy. *Atmospheric Meas.*
496 *Tech.*, **7**, 3295–3305.
- 497 Warneke, T., C. Petri, J. Notholt, and M. Buschmann, 2022: TCCON data from Orléans (FR),
498 Release GGG2020.R0. <https://doi.org/10.14291/tccon.ggg2020.orleans01.R0>.



- 499 Wennberg, P. O., C. M. Roehl, D. Wunch, J.-F. Blavier, G. C. Toon, N. T. Allen, R. Treffers,
500 and J. Laughner, 2022a: TCCON data from Caltech (US), Release GGG2020.R0.
501 <https://doi.org/10.14291/tccon.ggg2020.pasadena01.R0>.
- 502 Wennberg, P. O., D. Wunch, C. M. Roehl, J.-F. Blavier, G. C. Toon, and N. T. Allen, 2022b:
503 TCCON data from Lamont (US), Release GGG2020.R0.
504 <https://doi.org/10.14291/tccon.ggg2020.lamont01.R0>.
- 505 Wu, J., and Coauthors, 2021: Disentangling climatic and anthropogenic contributions to
506 nonlinear dynamics of alpine grassland productivity on the Qinghai-Tibetan Plateau. *J.*
507 *Environ. Manage.*, **281**, 111875, <https://doi.org/10.1016/j.jenvman.2020.111875>.
- 508 Wunch, D., and Coauthors, 2011: The total carbon column observing network. *Philos. Trans. R.*
509 *Soc. Math. Phys. Eng. Sci.*, **369**, 2087–2112.
- 510 Wunch, D., and Coauthors, 2017: Comparisons of the orbiting carbon observatory-2 (OCO-2) X
511 CO 2 measurements with TCCON. *Atmospheric Meas. Tech.*, **10**, 2209–2238.
- 512 Yang, and Coauthors, 2020: New ground-based Fourier-transform near-infrared solar absorption
513 measurements of XCO_2 , XCH_4 and XCO at Xianghe, China.
514 *Earth Syst. Sci. Data*, **12**, 1679–1696, <https://doi.org/10.5194/essd-12-1679-2020>.
- 515 Yang, Z., G. C. Toon, J. S. Margolis, and P. O. Wennberg, 2002: Atmospheric CO₂ retrieved
516 from ground-based near IR solar spectra. *Geophys. Res. Lett.*, **29**, 53–1.
- 517 Zhang, G., Z. Nan, L. Zhao, Y. Liang, and G. Cheng, 2021: Qinghai-Tibet Plateau wetting
518 reduces permafrost thermal responses to climate warming. *Earth Planet. Sci. Lett.*, **562**,
519 116858, <https://doi.org/10.1016/j.epsl.2021.116858>.
- 520 Zhang, Y., and Coauthors, 2015: Effects of grazing and climate warming on plant diversity,
521 productivity and living state in the alpine rangelands and cultivated grasslands of the
522 Qinghai-Tibetan Plateau. *Rangel. J.*, **37**, 57–65.
- 523 Zhou, M., and Coauthors, 2016: Validation of TANSO-FTS/GOSAT XCO₂ and XCH₄ glint
524 mode retrievals using TCCON data from near-ocean sites. *Atmospheric Meas. Tech.*, **9**,
525 1415–1430.
- 526 Zhou, M., and Coauthors, 2018: Atmospheric CO and XCH_4 time series and seasonal
527 variations on Reunion Island from ground-based in situ and FTIR (NDACC and TCCON)
528 measurements. *Atmospheric Chem. Phys.*, **18**, 13881–13901, <https://doi.org/10.5194/acp-18-13881-2018>.
- 530 Zhou, M., P. Wang, N. Kumps, C. Hermans, and W. Nan, 2022: TCCON data from Xianghe,
531 China, Release GGG2020.R0. <https://doi.org/10.14291/tccon.ggg2020.xianghe01.R0>.
- 532 Zhou, M., and Coauthors, 2023: Ground-Based Atmospheric CO₂, CH₄, and CO Column
533 Measurements at Golmud in the Qinghai-Tibetan Plateau and Comparisons with



534 TROPOMI/S5P Satellite Observations. *Adv. ATMOSPHERIC Sci.*, **40**, 223–234,
535 <https://doi.org/10.1007/s00376-022-2116-0>.

536